Journal of Rock Mechanics and Geotechnical Engineering 10 (2018) 740–752

Contents lists available at ScienceDirect

Journal of Rock Mechanics and Geotechnical Engineering

journal homepage: www.rockgeotech.org

Full Length Article

Constitutive model for monotonic and cyclic responses of loosely cemented sand formations

Mojtaba Rahimi [a,*], Dave Chan [b,c], Alireza Nouri [b]

[a] Department of Mechanical Engineering, Azad University, Khomeinishahr Branch, Isfahan, Iran
[b] Department of Civil and Environmental Engineering, University of Alberta, Edmonton, T6G 2W2, Canada
[c] China Three Gorges University, Yichang, China

ARTICLE INFO

Article history:
Received 28 August 2017
Received in revised form
18 December 2017
Accepted 5 January 2018
Available online 8 June 2018

Keywords:
Cyclic loading
Monotonic loading
Cemented sand
Plasticity
Constitutive model

ABSTRACT

This paper presents a model to simulate the monotonic and cyclic behaviours of weakly cemented sands. An elastoplastic constitutive model within the framework of bounding surface plasticity theory is adopted to predict the mechanical behaviour of soft sandstone under monotonic and cyclic loadings. In this model, the loading surface always passes through the current stress state regardless of the type of loading. Destruction of the cementation bonds by plastic deformation in the model is considered as the primary mechanism responsible for the mechanical degradation of loosely cemented sands/weak rock. To model cyclic response, the unloading plastic and elastic moduli are formulated based on the loading/reloading plastic and elastic moduli. The proposed model was implemented in FLAC2D and evaluated against laboratory triaxial tests under monotonic and cyclic loadings, and the model results agreed well with the experimental observations. For cyclic tests, hysteresis loops are captured with reasonable accuracy.

1. Introduction

This paper focuses on the constitutive model and degradation behaviour of cemented sand/soft sandstone under monotonic and cyclic loadings. Two main approaches for the study of weak sandstone degradation behaviour caused by repeated loading include laboratory testing by conducting cyclic loading tests and the development of cyclic plasticity theories. The majority of the studies in the area of cyclic loading of sandstone or cemented sand are limited to earthquake (dynamic) type of loading. Few studies have characterized the deformation properties of sandstone under slow cyclic loading both theoretically and experimentally. In general, the behaviour of geomaterials under cyclic loading is remarkably complex. This may be due to the dependence of the constitutive relationship on pressure and void ratio as well as the nonlinear behaviour of the sand matrix (Russell and Khalili, 2004; Khalili et al., 2005, 2006). Even the most sophisticated models cannot provide accurate predictions under general cyclic loading (O'Reilly and Brown, 1991). Therefore, development of a reliable model to capture the cyclic behaviour of geomaterials has become one of the most challenging issues in constitutive modelling (Vermeer and de Borst, 1984).

Most models for slow cyclic loading have been proposed for cohesionless soils and few studies have been conducted on sandstone behaviour in response to slow cyclic loading. Thus a model that could capture soft sandstone response under slow cyclic loading would be a significant advancement. The particular difficulty in the integration of the critical state concept in cyclic modelling is noted in the literature (Imam and Chan, 2008). In this paper, a critical state constitutive model is presented for slow cyclic loadings for soft sandstone.

The traditional plasticity theory appears to be unsuitable for modelling cyclic loading since it predicts a purely elastic response during unloading and reloading within the yield surface. That is, no plastic deformation is predicted for unloading and reloading unless the stress path reaches the yield surface again (Chen and Han, 2007). This is not suitable for modelling cyclic loading because, in reality, all unload-reload cycles result in the gradual accumulation of plastic strain and energy dissipation (Khong, 2004; Lenart, 2008) as shown schematically in Fig. 1. In other words, the response in

* Corresponding author.
E-mail addresses: rahimi2726@gmail.com, rahimi@iaukhsh.ac.ir (M. Rahimi).
Peer review under responsibility of Institute of Rock and Soil Mechanics, Chinese Academy of Sciences.

https://doi.org/10.1016/j.jrmge.2018.01.010

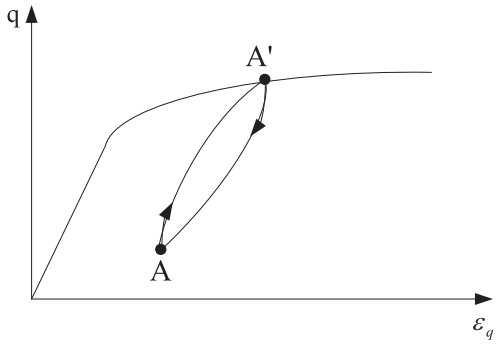

Fig. 1. Unloading and reloading from an elastoplastic state: perfect hysteresis loop in a complete cycle.

Fig. 1 suggests that the loading and unloading stress paths are not the same. This is known as hysteresis, and it shows that the material fails to recover all the energy it receives in the loading–unloading cycle (O'Reilly and Brown, 1991). This is attributed to energy dissipation due to plastic deformation (Lenart, 2008). Hysteresis is the result of non-uniform deformation of the material in which different parts of the material are undergoing different stages of loading and unloading.

The effect of non-uniform deformation at different stages of loading and unloading can be illustrated using a friction block model. Uniform deformation is analogous to a single block as shown in Fig. 2. In this case, there is only one displacement in the system, which is represented by u. There is no slipping until the horizontal force (T) reaches the maximum frictional force (F_k) when the block starts to move. At some displacement (u_1), if T decreases below F_k, movement will cease immediately and the force will vary between zero and F_k. There is no movement until T reaches F_k again and the displacement will continue from u_1. There is no hysteresis effect, and there is no study reported during the unloading and reloading cycle at u_1.

Non-uniform deformation in a material can be conceptually represented by a series of blocks as shown in Fig. 3. In this case, four blocks are connected by three springs with stiffness (K), and each block also is subjected to a normal force (N). The horizontal force (T) is slowly increased until the first block on the right, block 4, starts to move. There is no horizontal force applied on the other blocks until the spring between blocks 4 and 3 starts to compress. The force that will transmit to block 3 will be equal to the difference between T and F_k, where F_k is the frictional resistance at the base of each block. Again, there is no force applied on block 2 until the force in the spring between blocks 4 and 3 exceeds F_k in block 3. The process continues until all of the blocks start to move when T is equal to or exceeds $4F_k$. Since the movement of all the blocks is in the direction of T, F_k will be acting in the opposite direction (Fig. 3a).

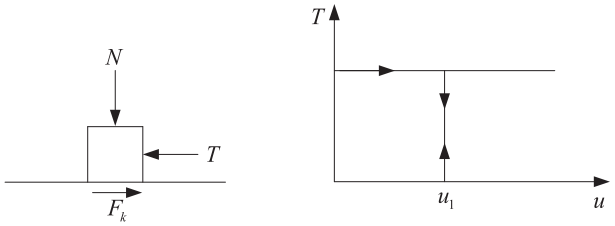

Fig. 2. Single frictional block on a flat surface and corresponding force-displacement response.

If T decreases below $4F_k$ after some movement of the blocks, the frictional force on block 4 will start to decrease until the direction is reversed as shown in Fig. 3b. There is no movement of block 4 until T decreases below $2F_k$. In this case, the force in the spring between blocks 4 and 3 will also decrease until the direction of the frictional force under block 2 reverses its direction. In this case, T will become zero, representing a fully unloaded state as shown in Fig. 3c.

If T increases again, there is no movement in block 4 until its frictional force changes its direction and the value of T is equal to $2F_k$ as shown in Fig. 3d. This represents that the reloading stage after T has been fully unloaded. It is clear that the reloading path is different from the unloading path since the mobilization of the frictional force under the blocks is different, unlike the case of a single block. Movement of block 4 occurs when T increases above $2F_k$. When T is equal to $4F_k$, the frictional forces under all of the blocks point in the same direction and movement will continue in the direction of T. Fig. 4 shows force-displacement response of block 4.

As demonstrated in this simple system of blocks, the hysteresis effect is a result of non-uniform mobilization of frictional forces under the blocks since they are connected by deformable springs. If the blocks are connected by rigid springs, the hysteresis effect will disappear.

In the case of a real material, since the stresses and strains in the material are generally non-uniform at the mesoscopic scale, it will give rise to the hysteresis effect much like the series of blocks connected by deformable springs. Therefore, energy dissipation occurs during the unloading and reloading process below the latest yield point.

The shortcomings of the classical plasticity theory led to extensive research, beginning in the 1960s, on developing more sophisticated plasticity models to capture the cyclic behaviour of geomaterials (Yu, 2006). Advanced constitutive models that have been introduced within the plasticity framework include multi-surface plasticity (Iwan, 1967; Mroz, 1967; Mroz et al., 1978, 1979), bounding surface plasticity (Dafalias and Popov, 1975; Krieg, 1975; Dafalias, 1982, 1986; Bardet, 1986; Khong, 2004; Khalili et al., 2005, 2006; Yang et al., 2011), generalized plasticity (Zienkiewicz et al., 1985; Pastor et al., 1985, 1990; Ling and Yang, 2006; Chung, 2010), and subloading surface plasticity (Hashiguchi, 1989; Hashiguchi and Chen, 1998).

Note that for our target material (i.e. naturally or artificially cemented sand), few constitutive models have been developed to simulate cyclic behaviour. For instance, Weng and Ling (2012) and Weng (2014) proposed their constitutive models based on generalized plasticity theory and verified their models against laboratory one-way cyclic loading of sandstone. Tariq and Maki (2012) conducted one-way cyclic loading tests on artificially cemented sand. However, they did not develop any constitutive model to simulate their experimental observations. Zhang et al. (2013) conducted one-way cyclic loading tests on a specific sandstone known as red sandstone. However, their proposed elastoplastic constitutive model was not verified against cyclic shear stress tests. Fu et al. (2014) developed a constitutive model within the framework of generalized plasticity and verified their model against experimental observations of one-way cyclic loading of rufous sandstone. Liu et al. (2016) conducted several laboratory one-way cyclic loading tests on structured (i.e. cemented) soils. However, they did not suggest any constitutive model to simulate experimental results.

The aim of this paper is to present a continuum elastoplastic constitutive model within the framework of bounding surface plasticity to model cyclic loading of frictional and cohesive material. A critical state constitutive model proposed by Imam (1999) and

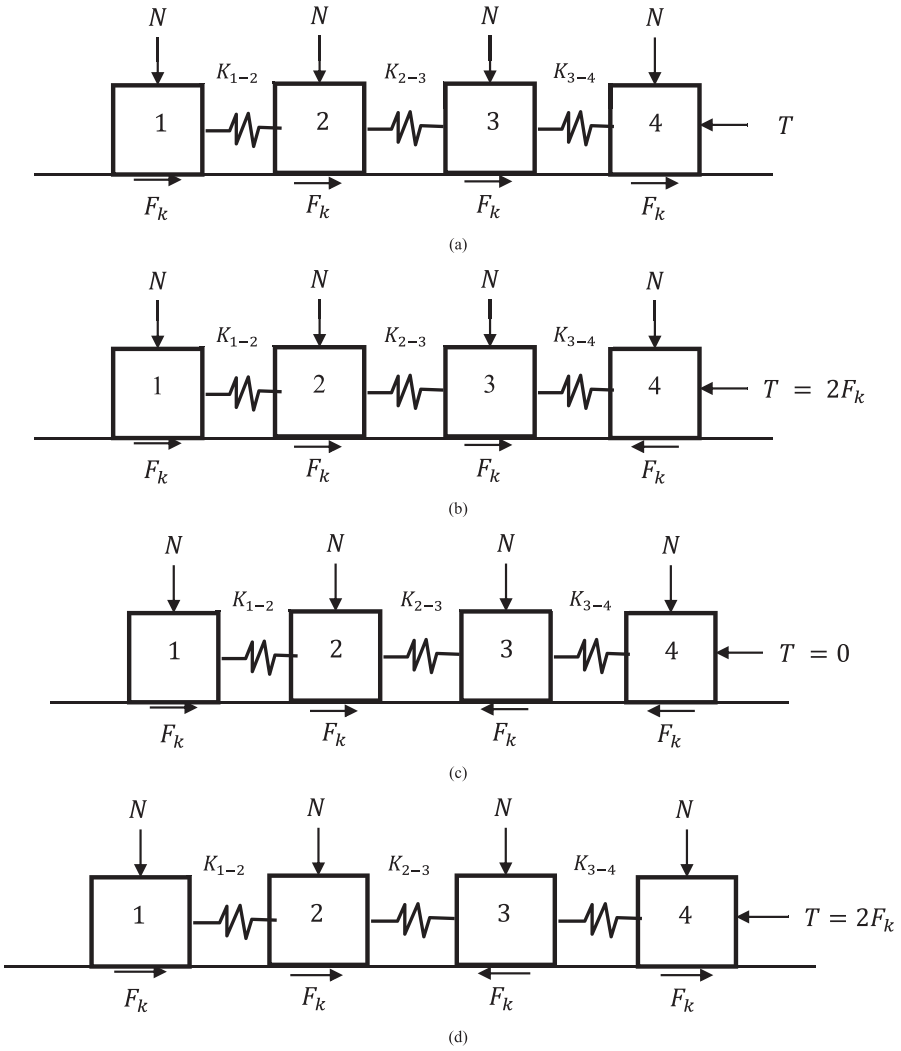

Fig. 3. (a) Four blocks in series where T is increased until movement occurs in all of the blocks; (b) T is decreased until the block 4 starts to move to the right; (c) T decreases to zero during unloading; and (d) T increases during reloading.

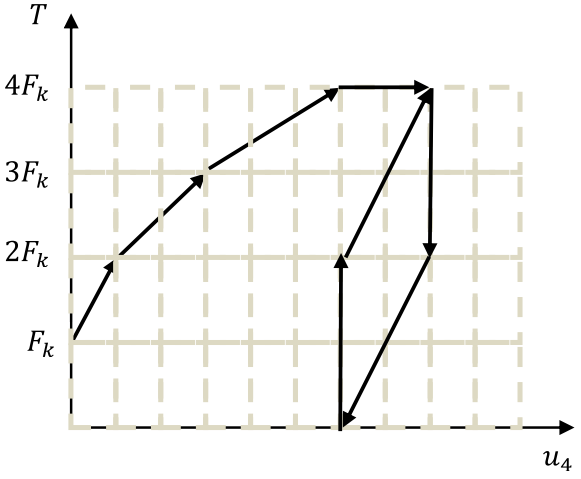

Fig. 4. Force-displacement response of block 4 in the four-block system connected by springs.

Imam et al. (2005) is chosen to be the base model. This model was developed for simulating the behaviours of cohesionless sands under monotonic loading. Thus, modifications are incorporated into the model to include the behaviour of cemented sand/soft sandstone under monotonic loading. To predict cyclic behaviour using the bounding surface plasticity theory, normalized plastic and elastic moduli are modified under unloading conditions without using the mapping rule. Although the projection rule is not incorporated, concepts of the bounding surface plasticity theory are used in the sense that plastic deformation is recorded for both loading and unloading conditions. This implies that the loading surface always passes through the current stress state regardless of the position of the stress path or the type of loading. Also by assuming a fixed size ratio between the bounding surface and the loading surface throughout the shearing process, the current stress always lies inside the bounding surface. However, unlike conventional bounding surface plasticity in which the plastic modulus is expressed as the summation of the additive and bounding surface plastic moduli, the plastic modulus is stated only as a function of that of the loading surface. This is similar to Imam and Chan (2008) approach for modelling the behaviour of cohesionless sand under cyclic loading. The proposed modified model ultimately is implemented in FLAC2D.

2. Cemented sand

Cemented soils and weak rocks constitute an intermediate class of geomaterials from a mechanical standpoint and are classified between soil and rock. They are often considered as non-textbook materials (Schnaid et al., 2001). Their mechanical behaviour under various conditions is not as well understood as those of hard rocks or soils. It is known, for example, that their strength and deformation characteristics show strong nonlinearity. Therefore, nonlinear elasticity models are more appropriate than linear elasticity models for soft rocks (Yoshinaka et al., 1998).

Cementation in naturally cemented sand originates from the precipitation of cementing agents like silica, carbonate minerals (especially calcite), clay minerals and iron oxides onto the surface of sand particles (Clough et al., 1981; Fjaer et al., 2008).

Cementation in artificially cemented sand comes from an externally added cementing agent such as Portland cement (Consoli et al., 2012). With an increase in the degree of cementation, peak strength, cohesion, tensile strength and stiffness of the material increase, while strain at peak strength decreases. Although a rise in the friction angle due to the addition of cementation has been reported, there is no agreement on the effect of cementation on the peak friction angle of the material. Some researchers believe that cementation causes no change to the friction angle. A list of different researchers who concluded different results on the effect of cementation on peak friction angle can be found in Abdulla and Kiousis (1997) and Schnaid et al. (2001). Cementation also gives rise to a more brittle response (Clough et al., 1981) and is more important than friction at low confining pressures. The failure mode is believed to be brittle for weakly cemented sand at lower confining pressures and ductile at higher pressures (see Fig. 5). Therefore, cemented sand shows a brittle response due to brittle failure of cementation bonds. At higher confining pressures, the frictional component is more dominant, resulting in a more ductile response. However, Fig. 6 suggests that for strongly cemented sand, cementation provides noticeable resistance even at higher confining pressures (Clough et al., 1981). Note that artificially cemented sands are usually considered as the better choice for conducting triaxial tests for constitutive model development because of their uniformity, homogeneity and reproducibility (Mohsin, 2008).

It is believed that the shear stress–strain curve for (artificially or naturally) cemented sand will eventually approach that for uncemented sand at a critical state which is associated with zero dilatancy rate (see Fig. 7). This, however, does not always occur since cementation may not be completely broken even after large amounts of shearing far beyond the initial yield point (Lee et al., 2004). That is, cemented sand after large amounts of shearing may arrive at the ultimate void ratio instead of the critical state void ratio which is associated with constant volume and is independent of the initial state. This implies that the concept of a unique critical state line (CSL) does not apply for (artificially or naturally) cemented sand because the CSL depends on the initial condition and especially on the cement contents. This is one of the most crucial challenges in applying the critical state theory to cemented sand. Experimental determination of the CSL for cemented sand is also difficult due to its brittle behaviour and strain localization (Marri, 2010).

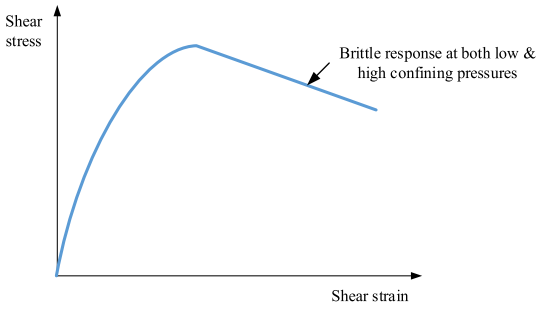

Fig. 6. Failure mode for strongly cemented sand.

3. Brief review of the original model

The detailed description of the original model can be found in Imam (1999) and Imam et al. (2005). A brief description is provided here.

The CSL in many proposed constitutive models for sand is used as a reference state to which various states of the soil are compared. Difficulty in determining the CSL position and the uncertainty of its position when the soil is loaded in different directions of shearing are the major setbacks for this approach. Errors in the determination of the CSL in these models can result in inaccuracies in the predicted behaviour (Imam, 1999; Imam et al., 2005). The proposed constitutive model also relies on the CSL position to determine the soil state at large strain. However, the impact of the uncertainties in the CSL location on soil properties at smaller strains is compensated by measuring the important properties under different directions of shearing from the experiment and correlating these properties to the CSL (Imam, 1999). The stress ratio at the peak of the undrained effective stress path (UESP) is one of these properties by which the stress ratio at the peak of the yield surface is predicted (Imam et al., 2002). Shear strains associated with the peak of the UESP are relatively small, implying that the measurement of this property is more reliable because strain in the early stages of the undrained tests is more uniform and less affected by localization (Imam, 1999; Imam et al., 2005). Fig. 8 illustrates typical UESP in monotonic

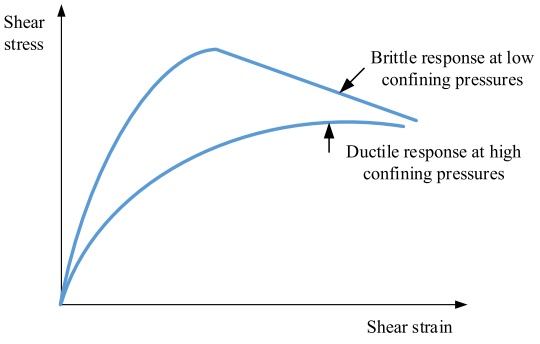

Fig. 5. Failure mode for weakly cemented sand.

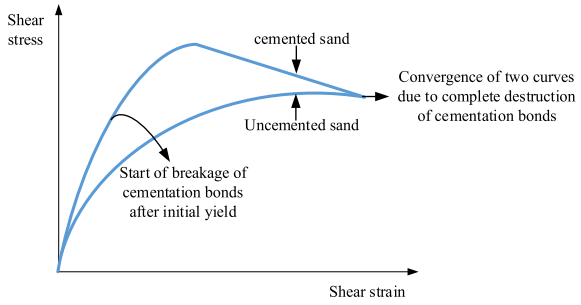

Fig. 7. Convergence of the shear stress–strain curves for uncemented and cemented sands (ideal case).

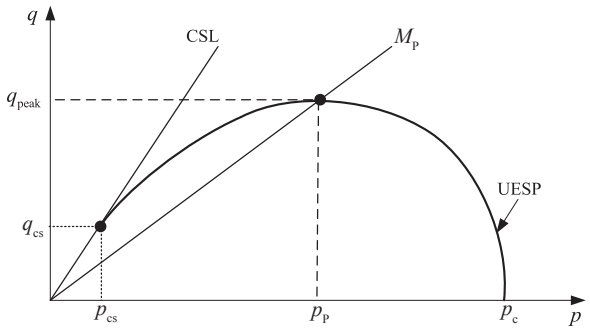

Fig. 8. Typical UESP in monotonic triaxial compressive loading on loose sands.

triaxial compressive loading on loose sands. The deviatoric stress initially increases until it reaches a peak at point $(p_p,\ q_{peak})$, where stress ratio M_p is mobilized. The deviatoric stress then decreases (strain softening) until UESP reaches the CSL (Imam et al., 2005).

The yield function of the original model is expressed as (Rahimi et al., 2015)

$$f = (\eta - \alpha)^2 - M_\alpha^2\left(1 - \sqrt{p/p_c}\right) = 0 \tag{1}$$

$$M_\alpha^2 = (5M_p - \alpha)(M_p - \alpha) \tag{2}$$

where η is the stress ratio, M_p is the stress ratio at the peak of UESP, p is the mean effective stress, α is a scalar which represents anisotropic consolidation and its magnitude is zero for isotropic consolidation, and p_c is the effective preconsolidation pressure which is considered as hardening parameter.

The parameter M_p is calculated for compressive and extensive loading, respectively, as follows (Rahimi et al., 2016):

$$M_{p,c} = \frac{6\sin\varphi_{p,c}}{3 - \sin\varphi_{p,c}} \tag{3}$$

$$M_{p,e} = \frac{6\sin\varphi_{p,e}}{3 + \sin\varphi_{p,e}} \tag{4}$$

where $\varphi_{p,c}$ and $\varphi_{p,e}$ are the friction angles at the peak of UESP in triaxial compression and triaxial extension, respectively. They are evaluated by (Imam et al., 2005):

$$\sin\varphi_{p,c} = \sin\varphi_\mu - k_p\psi_p \tag{5}$$

$$\sin\varphi_{p,e} = \sin\varphi_\mu - k_p\psi_p - a_p \tag{6}$$

where $\psi_p = e - e_p$ is the state parameter at the peak in which e is the void ratio, and e_p is the critical state void ratio which is evaluated at mean effective stress corresponding to M_p (i.e. at $p = p_p$); φ_μ is the friction angle associated with $\psi_p = 0$ in triaxial compression and is close to the interparticle friction angle; and k_p and a_p are the model parameters. Experimental observations which support the dependency of M_p to void ratio and the state parameter at the peak can be found in Imam et al. (2002). Note that the deviatoric stress (q) and the deviatoric strain (ε_q) are both positive under triaxial compression while they are both negative under triaxial extension.

When the stress path is at the peak of UESP, it is found from Eq. (1) that $p_p = 0.64\,p_c$ for isotropically consolidated sands regardless of void ratio and confining pressure at consolidation. This relationship is similar to that obtained by Ishihara (1993), who observed that the ratio of mean normal stress at the peak of UESP to that at consolidation is constant. By conducting undrained tests on sands consolidated to different mean normal stresses and void ratios, he obtained the ratios of 0.61 and 0.63 for clean and silty sands, respectively (Imam et al., 2005).

Isotropic nonlinear elasticity is adopted in the original model as

$$G = G_a\frac{(2.973 - e)^2}{1 + e}\left(\frac{p}{p_{atm}}\right)^{0.5} \tag{7}$$

$$K = K_a\frac{(2.973 - e)^2}{1 + e}\left(\frac{p}{p_{atm}}\right)^{0.5} \tag{8}$$

where K and G are the bulk and shear elastic moduli, respectively; G_a and K_a are the respective reference moduli associated with the atmospheric pressure p_{atm}; and e is the void ratio.

Following the work of Wood (1990) and Manzari and Dafalias (1997), the stress–dilatancy relationship is defined as (Rahimi et al., 2017):

$$D = A(M_{PT} - \eta) \tag{9}$$

$$A_c = \frac{9}{9 + 3M_{PT,c} - 2M_{PT,c}\eta} \tag{10}$$

$$A_e = \frac{9}{9 - 3M_{PT,c} - 2M_{PT,c}\eta} \tag{11}$$

where

$$\sin\varphi_{PT,c} = \sin\varphi_{cs} + k_{PT}\psi_s \tag{12}$$

$$\sin\varphi_{PT,e} = \sin\varphi_{cs} + k_{PT}\psi_s + a_{PT} \tag{13}$$

where D is the dilatancy rate, M_{PT} is the phase transformation stress ratio, φ_{cs} is the critical state friction angle, $\psi_s = e - e_{cs}$ is the state parameter (Been and Jefferies, 1985; Jefferies, 1993), e_{cs} is the critical void ratio, and k_{PT} and a_{PT} are both model parameters.

Similar to how M_p is calculated using $\sin\varphi_p$ under triaxial compression and extension conditions, M_{PT} values under compression and extension conditions are obtained from $\sin\varphi_{PT}$. Note that Eqs. (12) and (13) are similar to the relationship of Manzari and Dafalias (1997). Hardening in this model depends on the proximity to the critical state, in contrast to conventional critical state models which relate the size of the yield surface to void ratio (Jefferies, 1993). Shear hardening law is expressed as (Imam, 1999):

$$\frac{\partial p_c}{\partial \varepsilon_q^p} = \frac{hG_{ini}}{\left(p_f - p_c\right)_{ini}}\left(p_f - p_c\right) \tag{14}$$

where ε_q^p is the deviatoric plastic strain; h is a material parameter; p_f is the failure mean effective stress; and $(p_f - p_c)_{ini}$ and G_{ini} are the initial value of $p_f - p_c$ and the shear elastic modulus, respectively, at the end of consolidation. Calculation of M_f is based on $\sin\varphi_f$ $(M_f = 6\sin\varphi_f/(3 - \sin\varphi_f))$ which itself is obtained from the following equation (Imam, 1999):

$$\sin\varphi_f = \sin\varphi_{cs} - k_f\psi_s \tag{15}$$

where k_f is a material parameter.

4. A two-surface model for cemented sand

In line with the general tendencies to use as many simplifying assumptions as possible and to predict the stress–strain relationships using the simplest possible approach (Chen, 1994), a relatively simple constitutive model is presented. For modelling the mechanical behaviour of cemented sands, the base model is modified similar to the simplified assumptions made by Gens and Nova (1993). Gens and Nova (1993) and Nova (2005) suggested that a yield surface which had been originally proposed for cohesionless soils can be used for cemented soils after some modifications are made. They suggested that bonding (cementation between soil particles) provides tensile strength (p_t) and additional strength (p_o) to the material. In consideration of the additional strength, they suggested that the yield surface for the unbonded geomaterials must be enlarged towards the right. They also proposed that the yield surface must also be expanded towards the left to account for the tensile strength. Thus, more bonding leads to larger expansion of the yield surface towards both the right and left. Fig. 9 illustrates the schematic representation of the modified yield surface/loading surface. p_b controls the yielding of the bonded material in isotropic compression, which determines the size of the enlarged yield surface, and p_o controls the increase in the size of the initial elastic domain. The degree of bonding may be expressed as p_o/p_c (Gens and Nova, 1993).

To account for non-uniform deformation during cyclic loading, kinematic/anisotropic hardening parameters (i.e. p_a and q_a) are also integrated into the formula of the modified loading surface. Bounding and loading surfaces, elastic properties, flow rule, and stress–strain relationships are the major components of the modified model which are discussed herein.

4.1. Bounding and loading surfaces

The bounding and loading surfaces are assumed to have the same shape for simplicity. In terms of the conventional triaxial parameters, the bounding surface (F) and loading surface (f) can be written respectively as (see Fig. 10):

$$F = \left(\frac{\bar{q}-\bar{q}_a}{\bar{p}-\bar{p}_a+p_t}-\alpha\right)^2 - M_\alpha^2\left(1-\sqrt{\frac{\bar{p}-\bar{p}_a+p_t}{\bar{p}_b}}\right) = 0 \quad (16)$$

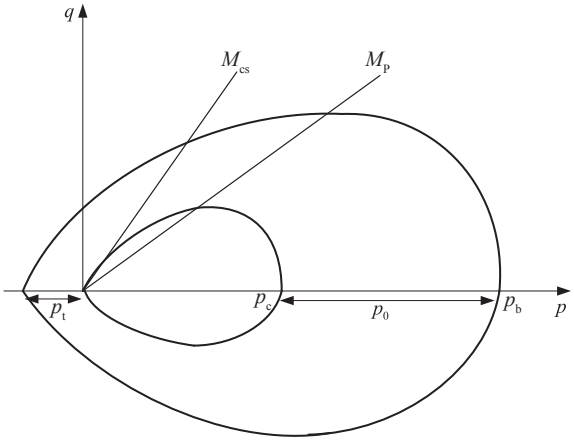

Fig. 9. Schematic representation of the modified yield surface.

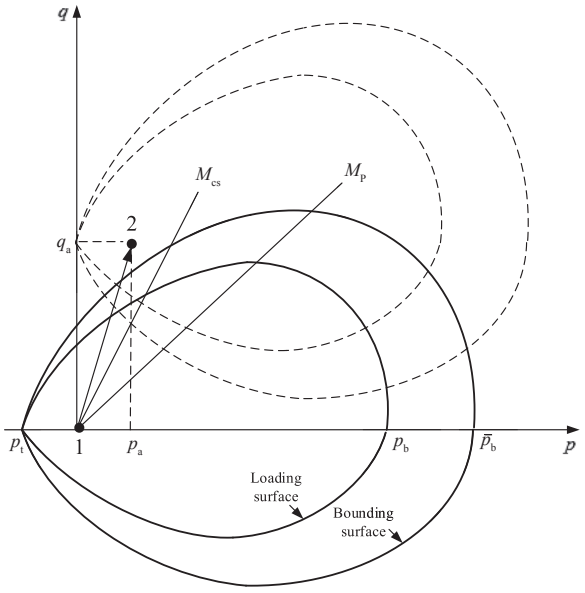

Fig. 10. Schematic representation of the loading and bounding surfaces at the start of loading (solid surfaces) and immediately after elastoplastic loading starts (dashed surfaces). In addition to change of position, size of two surfaces also changes with further elastoplastic loading (isotropic hardening). Kinematic hardening has been significantly magnified for better illustration.

$$f = \left(\frac{q-q_a}{p-p_a+p_t}-\alpha\right)^2 - M_\alpha^2\left(1-\sqrt{\frac{p-p_a+p_t}{p_b}}\right) = 0 \quad (17)$$

$$M_\alpha^2 = (5M_p-\alpha)(M_p-\alpha) \quad (18)$$

where q is the deviatoric stress, p_t is the tensile strength, and p_a and q_a are the components of the kinematic hardening tensor evolving with plastic strain. The kinematic hardening tensor is assumed to lie initially at the origin of the stress space, meaning the first time loading, i.e. $(p_a, q_a) = (0, 0)$. The superimposed bar denotes variables of the bounding surface.

To ensure that the current stress state will not cross the bounding surface, it is assumed that the initial ratio of size of the two surfaces remains constant during the shearing process. It is also assumed that the components of the kinematic hardening tensor always coincide with the two surfaces, i.e. $(p_a, q_a) = (\bar{p}_a, \bar{q}_a)$.

p_b and p_t are direct measures of the size of the loading surface and the tensile strength, respectively. They are defined using the following relationships:

$$p_b = p_c + (1+\beta)p_o \quad (19)$$

$$p_t = \beta p_o \quad (20)$$

where p_o is a measure of the increase in size of the uncemented yield surface due to strength increase by cementation, β is defined as the ratio between the tensile strength and p_o, and p_c plays the same role as the preconsolidation pressure for uncemented sand.

Destruction of the bonds between sand grains due to plastic deformation is assumed to lead to only the changes in the size of the loading and bounding surfaces. Their shapes, however, are supposed to remain unchanged. To consider this destruction process, the following simple linear relationship is assumed:

$$\mathrm{d}p_{\mathrm{o}} = -\gamma p_{\mathrm{o}} |\mathrm{d}\varepsilon_q^p| \tag{21}$$

where γ is a decay parameter which determines the rate of bond breakage, and $\mathrm{d}p_{\mathrm{o}}$ indicates the change in p_{o} due to the change in plastic shear strain.

Note that the origin of plastic deformation of sand under low shear stresses mainly comes from grain crushing at the particle contact. Gross slippage at the particle contact, however, is responsible for plastic deformation under high shear stresses because the mobilized shear stresses are sufficient to overcome the resistance of the contact (Imam, 1999).

The nonlinear kinematic hardening law of Armstrong and Frederick (1966) is adopted to control the evolution of the loading surface. For triaxial conditions, it is expressed as

$$\dot{p}_\alpha = \frac{2}{3} c_1 \frac{\dot{\varepsilon}_p^p}{3} - c_2 p_\alpha \dot{\omega} \tag{22}$$

$$\dot{q}_\alpha = c_1 \dot{\varepsilon}_q^p - c_2 q_\alpha \dot{\omega} \tag{23}$$

where c_1 and c_2 are the model constants; $\dot{\varepsilon}_q^p$ and $\dot{\varepsilon}_p^p$ are the plastic deviatoric and volumetric strain increments, respectively; and $\dot{\omega}$ is the accumulative plastic strain increment defined as

$$\dot{\omega} = \sqrt{\frac{2}{3}\dot{\varepsilon}_{ij}^p \dot{\varepsilon}_{ij}^p} \tag{24}$$

The parameters p_α and q_α are the components of the kinematic hardening tensor, which are defined for triaxial conditions as

$$p_\alpha = \frac{\alpha_{11} + 2\alpha_{33}}{3} \tag{25}$$

$$q_\alpha = \alpha_{11} - \alpha_{33} \tag{26}$$

4.2. Elastic properties

The definition of the elastic moduli in the original model is modified similar to Yu et al. (2007) approach as follows:

$$G = G_{\mathrm{a}} \frac{(2.973 - e)^2}{1 + e} \left[\frac{p}{p_{\mathrm{atm}}} \left(1 + \sqrt{p_{\mathrm{o}}/p} \right) \right]^{0.5} \tag{27}$$

$$K = K_{\mathrm{a}} \frac{(2.973 - e)^2}{1 + e} \left[\frac{p}{p_{\mathrm{atm}}} \left(1 + \sqrt{p_{\mathrm{o}}/p} \right) \right]^{0.5} \tag{28}$$

This definition provides two important features of the bonded geomaterials: (a) extra initial elastic stiffness due to bonding; and (b) the progressive reduction of elastic moduli due to the breakage of bonding during plastic straining (Yu et al., 2007).

The elastic properties for unloading conditions with a slight modification are given as

$$G = |\eta| G_{\mathrm{a}} \frac{(2.973 - e)^2}{1 + e} \left[\frac{p}{p_{\mathrm{atm}}} \left(1 + \sqrt{p_{\mathrm{o}}/p} \right) \right]^{0.5} \tag{29}$$

$$K = |\eta| K_{\mathrm{a}} \frac{(2.973 - e)^2}{1 + e} \left[\frac{p}{p_{\mathrm{atm}}} \left(1 + \sqrt{p_{\mathrm{o}}/p} \right) \right]^{0.5} \tag{30}$$

where $|\eta|$ denotes the absolute value of the stress ratio. Incorporation of η in the expression for the elastic moduli results in the prediction of a stiffer response at the commencement of unloading and then a softer response when the stress ratio approaches the smaller deviatoric stresses. The decreasing trend is particularly more pronounced when the deviatoric stress is very small (see Fig. 11). It should be noted that a decrease in η or q (usually accompanied with a decrease in deviatoric/axial strain) during compressive loading signifies the unloading conditions. Similarly, an increase in η or q (normally followed by an increase in deviatoric/axial strain) during compressive loading indicates the loading/reloading conditions.

Suggestion of these expressions for the unloading elastic moduli comes from experimental observations. That is, the stiffness shows a sudden increase immediately after the inception of unloading accompanied with a sudden decrease when soil undergoes further unloading (O'Reilly and Brown, 1991). The elastic moduli for reloading conditions, however, are assumed to remain the same as those of the original loading. Although assuming that the elastic properties of the reloading conditions are in the same form as those for unloading conditions leads to better predictions of the hysteresis loops (see Fig. 16), it results in numerical instabilities in this case in FLAC2D model.

4.3. Flow rule

Experimental observations suggest that dilatancy is affected by the degree of cementation between sand particles. Most of studies have shown that an increase in the cement content gives rise to an increase in dilatancy and subsequent decrease in compression (Clough et al., 1981; Marri, 2010). Therefore, the original Rowe's stress–dilatancy relationship proposed for cohesionless sands cannot provide a good description for calculating the rate of dilation of cemented sands/weak sandstone.

By incorporating cohesion for compression, Rowe's stress–dilatancy relationship can be calculated by (Yu et al., 2007; Rahimi, 2014; Rahimi et al., 2015):

$$D = \frac{9(M_{\mathrm{cs}} - \eta) + 6\frac{c}{p}\sqrt{(2M_{\mathrm{cs}} + 3)(-M_{\mathrm{cs}} + 3)}}{9 + 3M_{\mathrm{cs}} - 2M_{\mathrm{cs}}\eta + 4\frac{c}{p}\sqrt{(2M_{\mathrm{cs}} + 3)(-M_{\mathrm{cs}} + 3)}} \tag{31}$$

where D is the dilatancy rate, c is the cohesion, and M_{cs} is the critical state stress ratio. Cohesion is assumed to degrade with the total plastic strain increment as follows:

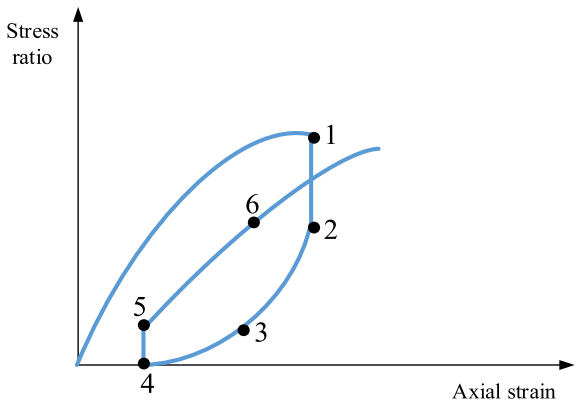

Fig. 11. Stress ratio vs. Axial strain. 1–2 shows a sudden increase in stiffness after start of unloading, 2–3 shows a sudden decrease when the material undergoes further unloading. 3–4 shows the softer response under unloading when the material approaches lower values of the stress ratio. 4–5 shows a sudden increase in stiffness after start of reloading. 5–6 shows softer response when the material is subjected to further reloading.

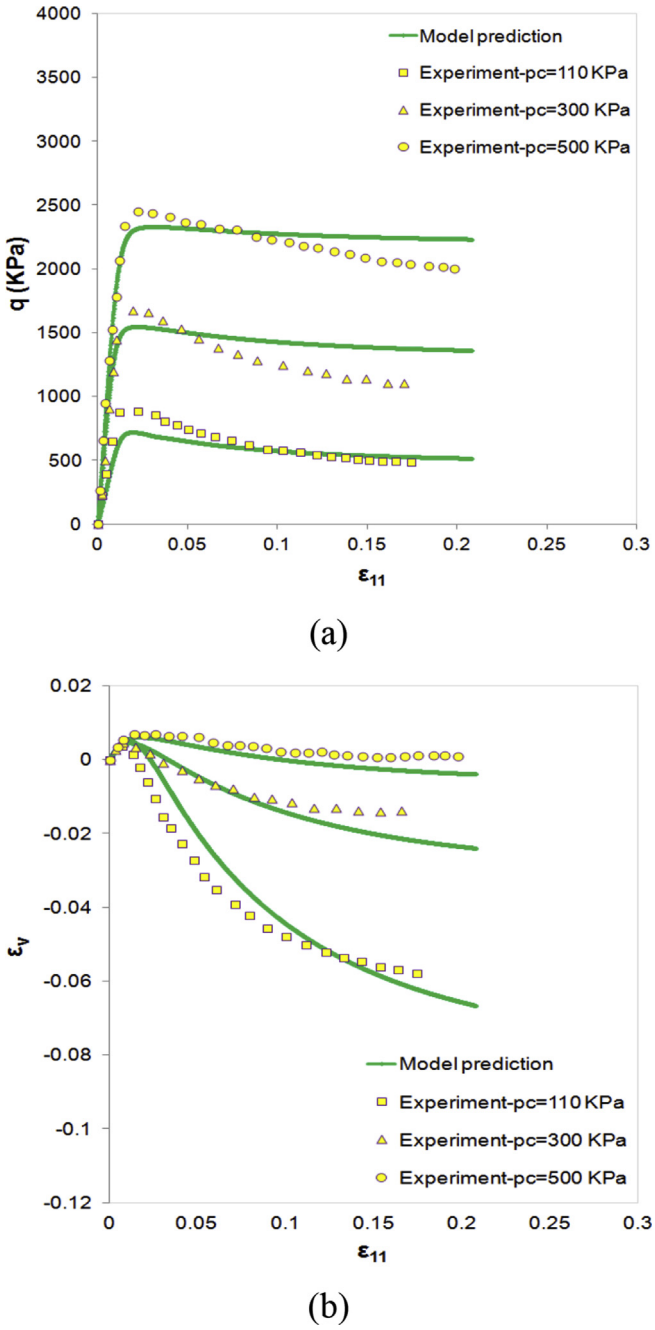

Fig. 12. Measured and predicted responses of Tehran Alluvium cemented sand with cement content of 3%.

$$dc = c\exp\left[-\xi\sqrt{\left(\dot{\varepsilon}_q^p\right)^2+\left(\dot{\varepsilon}_p^p\right)^2}\right] \tag{32}$$

where ξ indicates the rate of cohesion degradation.

Clearly, when cohesion approaches zero, the original Rowe's stress–dilatancy relationship for cohesionless soils is recovered. The plastic potential function (g) associated with the dilatancy relationship in Eq. (31) takes the form (Yu et al., 2007) as follows:

$$g = 3M_{cs}\ln\left(\frac{p+p_t-k_g}{\varphi_g}\right)+(2M_{cs}+3)\ln\left[\frac{2(q-h_g)}{p+p_t-k_g}+3\right] + (M_{cs}-3)\ln\left(3-\frac{q-h_g}{p+p_t-k_g}\right) = 0 \tag{33a}$$

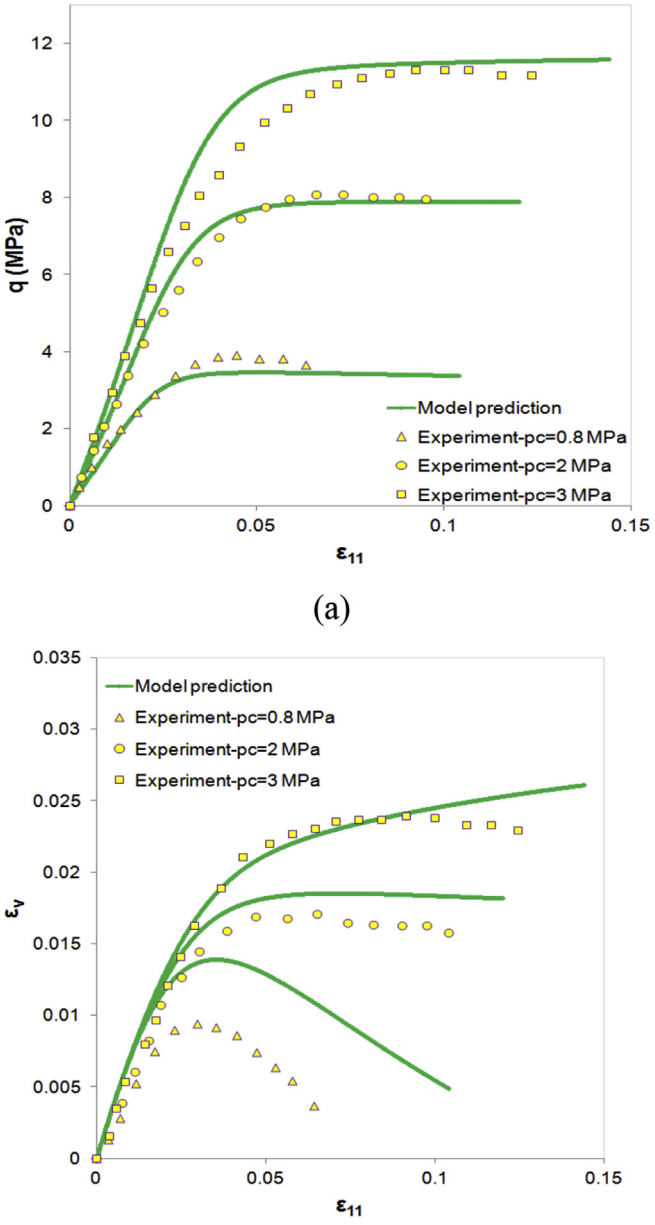

Fig. 13. Measured and predicted responses of a slightly weathered rock under monotonic loading.

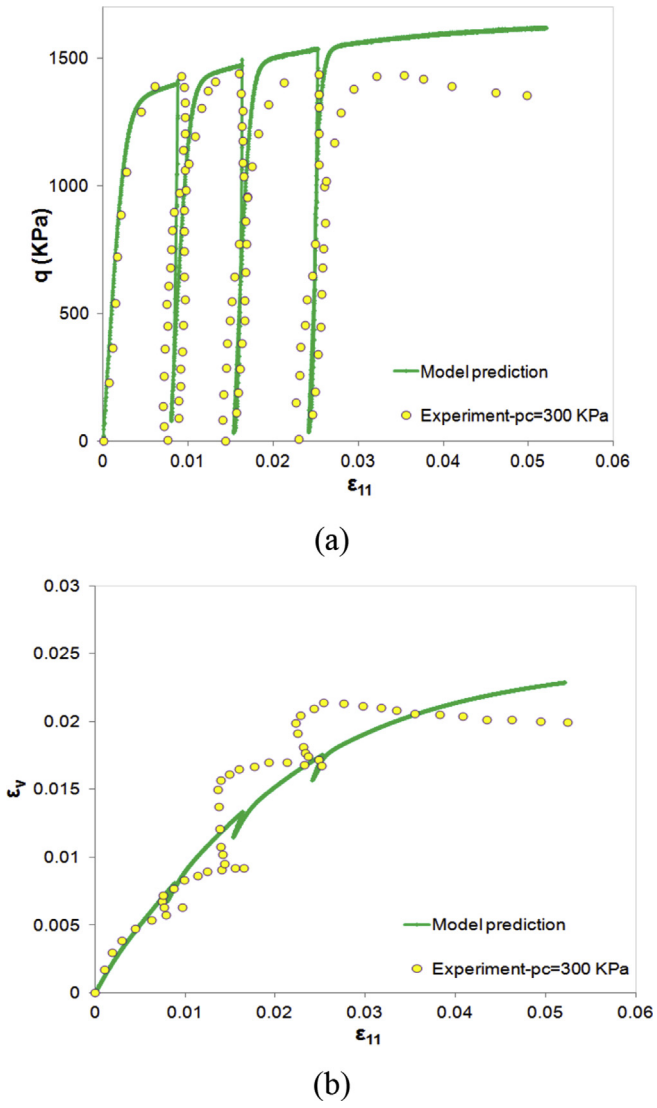

Fig. 14. Measured and predicted responses of a cemented carbonate sand in a triaxial drained cyclic compression test.

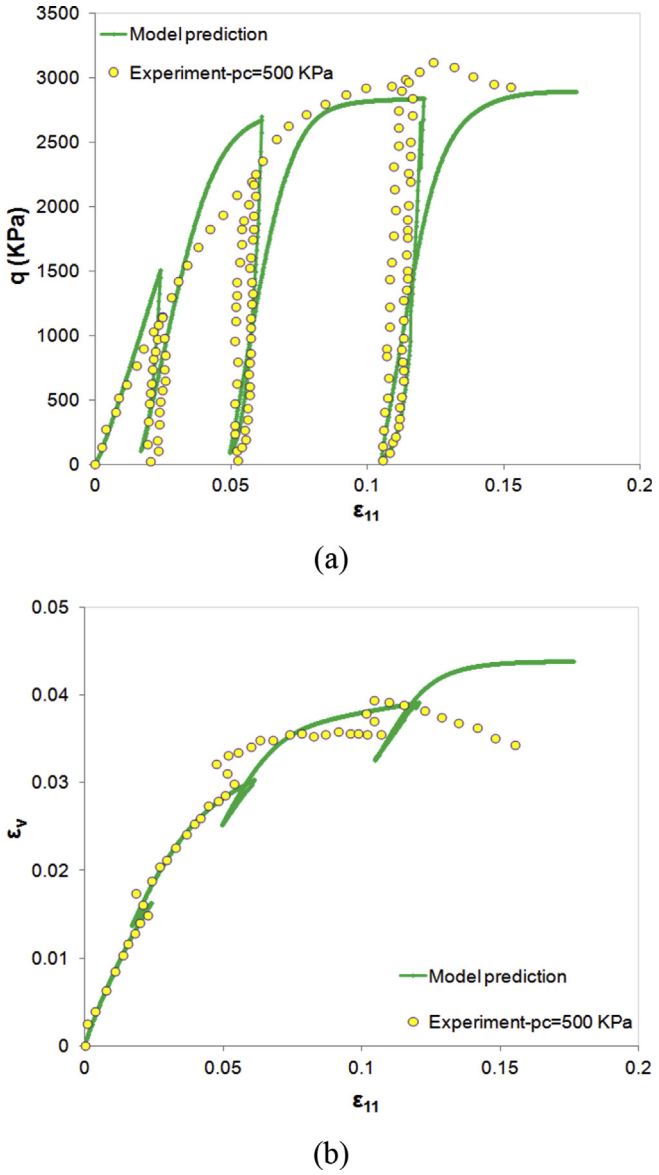

Fig. 15. Measured and predicted responses of rufous sandstone under a triaxial drained cyclic compression test.

$$k_g = \frac{\sqrt{(3+2M_{cs})(3-M_{cs})}\,(36-12M_{cs})\,c}{18M_{cs}^2-27M_{cs}-81} \tag{33b}$$

$$h_g = \frac{\sqrt{(3+2M_{cs})(3-M_{cs})}\,(-54+18M_{cs})\,c}{18M_{cs}^2-27M_{cs}-81} \tag{33c}$$

where φ_g can be determined for any given stress state (p,q) by solving equation Eq. (33a) (Yu, 2006).

Consistent with Imam (1999) and Imam et al. (2005), the flow rule is expressed based on a variable phase transformation stress ratio instead of a constant critical state stress ratio. Thus, for triaxial compression conditions, we have

$$D = \sqrt{\frac{2}{3}}\left[(M_{pt}-|\eta|)+\frac{6B}{C}\right] \tag{34}$$

$$A = \frac{9}{C} \tag{35}$$

$$C = 9+3M_{PT}-2M_{PT}|\eta|+4B \tag{36}$$

$$B = \frac{c}{p}\sqrt{(2M_{PT}+3)(-M_{PT}+3)} \tag{37}$$

where M_{PT} is the phase transformation stress ratio.

4.4. Stress–strain relationships

Constitutive equations are governed by the following equations in line with incrementally linear stress–strain relationships:

$$\dot{p} = K\left[\dot{\varepsilon}_p - LD\mathrm{sign}(m_p)\right] \tag{38}$$

$$\dot{q} = 3G\left[\dot{\varepsilon}_q - \sqrt{2/3}\,L\mathrm{sign}(m_q)\right] \tag{39}$$

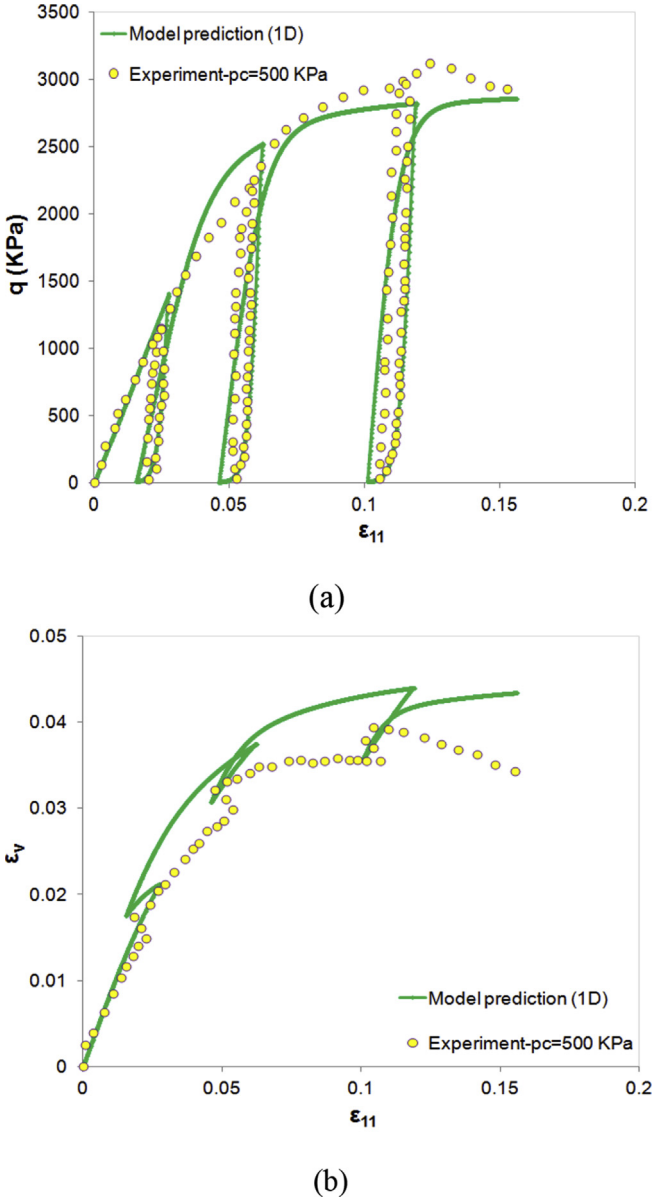

Fig. 16. Prediction of rufous sandstone behaviour using 1D model (reloading elastic moduli are defined similar to those of unloading conditions).

where m_p and m_q are the components of the unit vector normal to the plastic potential surface which are obtained using the dilatancy relationship. L is determined from the following relationship:

$$L = \frac{KR\dot{\varepsilon}_p + \sqrt{6}\,G\dot{\varepsilon}_q}{H_n + KRD\text{sign}(m_p) + 2G\text{sign}(m_q)} \tag{40}$$

$$R = \sqrt{\frac{2}{3}}\frac{\frac{\partial f}{\partial p}}{\left|\frac{\partial f}{\partial q}\right|} \tag{41}$$

$$\frac{\partial f}{\partial p} = \frac{-2}{p - p_a + p_t}\left[\left(\frac{q - q_a}{p - p_a + p_t}\right)^2 - \alpha\left(\frac{q - q_a}{p - p_a + p_t}\right)\right] + \frac{M_\alpha^2}{2\sqrt{p_b(p - p_a + p_t)}} = -\frac{\partial f}{\partial p_a} \tag{42}$$

$$\frac{\partial f}{\partial q} = \frac{2}{p - p_a + p_t}\left(\frac{q - q_a}{p - p_a + p_t} - \alpha\right) = -\frac{\partial f}{\partial q_a} \tag{43}$$

$$m_q = \frac{1}{\sqrt{1 + D^2}} \tag{44}$$

$$m_p = \begin{cases} \dfrac{tD}{\sqrt{1 + D^2}} & (D \geq 0) \\ \dfrac{-tD}{\sqrt{1 + D^2}} & (D < 0) \end{cases} \tag{45}$$

where $t = 1$ for compressive loading and $t = -1$ for extensive loading. For unloading, the components of the unit vector to the plastic potential surface are obtained by those defined already:

$$m_{p,u} = -m_p \tag{46}$$

$$m_{q,u} = m_q \tag{47}$$

H_n is the normalized plastic modulus which is obtained from the following equation:

$$H_n = -\sqrt{\frac{2}{3}}\frac{1}{\left|\frac{\partial f}{\partial q}\right|}\frac{\partial f}{\partial p_b}\frac{\partial p_b}{\partial \varepsilon_q^p} + H_n^{\text{kinematic}} \tag{48}$$

$$H_n^{\text{kinematic}} = R\left[\frac{2}{9}c_1 D\text{sign}(m_p) - c_2\, p_\alpha\sqrt{\frac{2}{9}D^2 + 1}\right] + c_1 - c_2 u_Q q_\alpha\sqrt{\frac{2}{9}D^2 + 1} \tag{49}$$

$$\frac{\partial f}{\partial p_b} = -\frac{M_\alpha^2}{2p_b}\sqrt{\frac{p - p_a + p_t}{p_b}} \tag{50}$$

$$\frac{\partial p_b}{\partial \varepsilon_q^p} = \frac{\partial p_c}{\partial \varepsilon_q^p} + (1 + \beta)\frac{\partial p_o}{\partial \varepsilon_q^p} = \frac{hG_{\text{ini}}}{\left(p_f - p_c\right)_{\text{ini}}}\left(p_f - p_c\right) - (1 + \beta)\gamma p_o \tag{51}$$

where p_f is the failure mean normal stress which is calculated using an iterative method from the following equation:

$$p_f = \frac{p - p_a}{\left[1 - \frac{\left(\frac{M_f p_f - q_a}{p_f - p_a} - \alpha\right)^2}{M_\alpha^2}\right]^2} \tag{52}$$

u_Q in Eq. (49) is defined as follows:

$$u_Q = \frac{\frac{\partial f}{\partial q}}{\left|\frac{\partial f}{\partial q}\right|} \tag{53}$$

H_n for unloading is assumed to be related to loading as follows:

$$\frac{H_{n,u}}{H_n} = R_u\sqrt{\frac{p}{p_{atm}}|\eta|} \tag{54}$$

where R_u is a model constant.

Due to the decrease in the stress ratio, higher plastic strains are predicted for a given total strain increment with advancement of

unloading during one-way cyclic loading, which is in accordance with experimental observations.

4.5. Material parameters

The parameters k_p, φ_μ, φ_{cs}, k_{PT}, G_a, K_a, h, k_f, and CSL are material parameters of the original model (Imam, 1999). Methods of determination of these parameters have been given in Imam et al. (2005). The following material parameters were introduced in the upgraded model:

(1) Initial value of p_o;
(2) Initial value of tensile strength to evaluate β;
(3) Decay parameter of bond strength (γ);
(4) Cohesion (c);
(5) Rate of degradation of cohesion (ξ);
(6) Anisotropic hardening parameters (c_1, c_2); and
(7) Ratio of unloading plastic modulus to that of loading (R_u).

The initial value of p_o is equal to the difference between the initial values of p_b and p_c. The initial value of p_c is obtained from the maximum mean normal stress characterizing the initial elastic domain for cohesionless soil. The initial value of p_b can be evaluated by conducting an isotropic compression test on weakly cemented sand to determine the initial yield value of p_b (Nova, 2005).

The parameter β is obtained using the initial value of the tensile strength. If there is no data regarding the tensile strength, the unconfined compressive strength can be used for an approximation of the tensile strength. The tensile strength is in order of 5%–20% of the unconfined compressive strength (Nova, 2005).

The parameter γ controls the rate at which bonds are broken. It is determined by fitting theoretical results to the experimental data in an isotropic compression test. The higher the γ value is, the faster the compression curve will become identical to that for uncemented material (Nova, 2005).

The parameter c can be evaluated using the loading function or Mohr-Coulomb yield function. The parameter ξ can be evaluated by fitting theoretical results of the volumetric behaviour to those of experimental observations.

The anisotropic hardening parameters c_1 and c_2 determine the contribution of anisotropic/kinematic hardening in the combined isotropic-kinematic/mixed hardening rule. Larger difference between c_1 and c_2 causes larger contribution of kinematic hardening to overall hardening. The constants c_1 and c_2 may be determined from stress–strain curve of uniaxial tests (Araujo, 2002; Dunne and Petrinic, 2005).

The parameter R_u is determined by fitting model predictions to unloading experimental data. A larger value of R_u results in a stiffer unloading response and a smaller unloading-induced plastic strain increment and vice versa.

4.6. Model performance

The performance of the proposed model is examined first against two sets of triaxial monotonic loading tests. Then, it is assessed against two triaxial one-way cyclic loading tests. All simulations performed by FLAC are based on axisymmetric conditions. Fig. 12 shows the calculated and observed behaviours of an artificially cemented gravelly sand under triaxial compression monotonic tests. Hydrated lime is used as the cementing agent for these samples (Asghari et al., 2003). Table 1 lists the material parameters used for these analyses. Due to the lack of data, some of the material parameters such as the CSL and φ_{cs} are selected based on the best match using one set of values for these parameters under a given cement content. Isotropic hardening is assumed for monotonic loading. Thus, a zero value is allocated for kinematic hardening related constants. The p_o value is assigned for different confining stresses under a given cement content such that a constant initial bonding is obtained.

Table 1
Material parameters used for calibration in Figs. 12 and 13 ($p^* = p + p_t$).

Parameter	Cemented gravelly sand (Fig. 12)	Weathered rock (Fig. 13)
k_p	1.5	1
φ_μ (°)	35	35
φ_{cs} (°)	43.5	41.5
k_{PT}	1	1
G_a (Pa)	2×10^7	9×10^6
K_a (Pa)	3×10^7	15×10^6
h	1	1
k_f	0.75	0.75
e_{cs}	$0.47 - 0.02\ln p^*$ (p^* in MPa)	$0.24 - 0.04\ln p^*$ (p^* in MPa)
p_o (Pa) (at highest p_c)	1.25×10^6	9×10^6
γ	25	15
c (Pa)	2×10^5	1×10^6
ξ	25	15
β	0.2	0.1

As seen in Fig. 12, the predicted and measured volumetric behaviours are in good agreement. The change of behaviour from contractive to dilative is observed in all tests. This is predicted numerically in the proposed model by a change of dilatancy rate from positive to negative. Fig. 12 also indicates less dilation at higher confining pressures as expected. Unlike volumetric behaviour, however, there is small discrepancy in the predicted and observed stress–strain behaviours. Using one critical state friction angle has led to slight underestimation of the peak deviatoric strength especially for the test with the confining pressure of 110 kPa, demonstrating the difficulty in applying the critical state theory for cemented soil. This difficulty has been observed experimentally as well. For instance, Lee et al. (2004) experimentally measured a larger critical state stress ratio and thus a greater critical state friction angle at lower confining pressures for a cemented soil with a given cement percentage.

Fig. 13 shows the predicted and observed behaviours of a slightly weathered rock obtained from the site of a pumped storage power station (Fu et al., 2014). The CSL and cohesion intercept are chosen based on the best match for the rock behaviour under various confining stresses due to lack of data. Isotropic hardening is assumed for the material behaviour under monotonic loading. The p_o value is also allocated in a way similar to the procedure mentioned for Tehran Alluvium cemented sand in Fig. 12. The material parameters used in Fig. 13 are listed in Table 1.

The model was next examined against the cyclic triaxial data (Mohsin, 2008) for a cemented carbonate sand with 20% gypsum content (gypsum was used as the cementing agent) and an initial dry unit weight of 13 kN/m^3 (see Fig. 14). The model is able to predict the narrow hysteresis loops, but the loops may not be shown clearly in Fig. 14. In this calculation, some of the material parameters were chosen based on the best match. Table 2 lists the material parameters used for the calibration of the triaxial cyclic and monotonic compression tests shown in Figs. 14–16.

The model was then assessed against cyclic triaxial data of the rufous sandstone, which is a slightly weathered rock (Fu et al., 2014). Due to the absence of required data, some material parameters are assigned to provide the best match to the observed behaviour. As can be seen from Fig. 15, the FLAC2D model is reasonably capable of capturing the observed shear and volumetric cyclic behaviours of the rufous sandstone. However, there is a discrepancy between the measured and predicted volume changes during unloading. Experimental observations show that the material contracts during unloading while the model predictions

Table 2
Material parameters used for calibration in Figs. 14–16 ($p^* = p + p_t$).

Parameter	Cemented carbonate sand (Fig. 14)	Rufous sandstone (Figs. 15 and 16)
k_p	1	1.25
φ_μ (°)	42	39
φ_{cs} (°)	47	47
k_{PT}	1	1.25
G_a (Pa)	2×10^8	4.5×10^6
K_a (Pa)	5×10^7	7.5×10^6
h	1	1
k_f	0.75	0.75
e_{cs}	$2.29 - 0.44 \log_{10} p^*$ (p^* in kPa)	$-0.0063477 p^{*3} + 0.0367 p^{*2} - 0.11991 p^* + 0.35$ (p^* in MPa)
p_o (Pa)	9×10^5	25×10^5
γ	15	20
c (Pa)	2×10^6	4×10^6
ξ	25	150
β	0.2	0.3
c_1	1×10^7	5×10^7
c_2	500	500
R_u	15	5

suggest that it undergoes expansion. However, in general, the measured and predicted volumetric behaviours are in relatively good agreement.

Fig. 16 shows the model predictions using one-dimensional (1D) model (i.e. the constitutive equations are solved for one node) for the same initial conditions and material parameters as those of Fig. 15, when reloading elastic moduli are assumed similar to the unloading elastic moduli (see Eqs. (29) and (30)). As observed, the hysteresis loops are captured better in this case using 1D model. However, discrepancy between the measured and predicted volumetric responses exists similar to Fig. 15. Note that numerical instabilities were encountered in the FLAC2D model when the reloading moduli were defined using Eqs. (29) and (30) rather than Eqs. (27) and (28). Therefore, to avoid the instability, the reloading elastic moduli were chosen to be the same as the loading elastic moduli (Eqs. (27) and (28)) in FLAC simulations.

5. Conclusions

A continuum elastoplastic constitutive model has been presented in this paper to investigate the degradation of weak artificially and naturally cemented sand under monotonic and one-way cyclic loadings. Destruction of bonds between sand particles due to plastic deformation has been considered as the reason for mechanical degradation under applied loads. Several triaxial monotonic and cyclic compression tests on both artificially and naturally cemented sands have been chosen to assess the model performance. A comparison between the predicted and observed behaviours shows reasonably fair agreement. Hysteresis loops have been captured with reasonable accuracy too. However, the observed softening response cannot be reproduced by the model well. Moreover, the increase in volumetric strain (i.e. further compaction) upon unloading cannot be modelled by the proposed constitutive model. Modification of the stress–dilatancy relationship under unloading conditions appears to be a potential candidate for addressing this shortcoming.

Conflicts of interest

The authors wish to confirm that there are no known conflicts of interest associated with this publication and there has been no significant financial support for this work that could have influenced its outcome.

Acknowledgements

Funding for this project has been provided by BP Canada and the Nature Science and Engineering Research Council of Canada (NSERC), for which the authors are grateful.

References

Abdulla AA, Kiousis PD. Behaviour of cemented sands – I. Testing. International Journal for Numerical and Analytical Methods in Geomechanics 1997;21(8):533–47.
Araujo MC. Non-linear kinematic hardening model for multiaxial cyclic plasticity [MSc Thesis]. Louisiana, USA: Louisiana State University; 2002.
Armstrong PJ, Frederick CO. A mathematical representation of the multiaxial Bauschinger effect. CEGB Report, RD/B/N731. Berkeley Nuclear Laboratories; 1966.
Asghari E, Toll DG, Haeri SM. Triaxial behaviour of a cemented gravely sand, Tehran alluvium. Geotechnical & Geological Engineering 2003;21(1):1–28.
Bardet JP. Bounding surface plasticity model for sands. Journal of Engineering Mechanics 1986;112(11):1198–217.
Been K, Jefferies MG. A state parameter for sands. Géotechnique 1985;35(2):99–112.
Chen WF. Constitutive equations for engineering materials. Netherlands: Elsevier; 1994.
Chen WF, Han DJ. Plasticity for structural engineers. New York: John Ross Publishing; 2007.
Chung AB. Unified modelling for sand under generalized stress paths [PhD Thesis]. New York, USA: Columbia University; 2010.
Clough GW, Shafii Rad N, Bachus RC, Sitar N. Cemented sands under static loading. Journal of the Geotechnical Engineering Division 1981;107(6):799–817.
Consoli NC, Cruz RC, da Fonseca AV, Coop MR. Influence of cement-voids ratio on stress-dilatancy behaviour of artificially cemented sand. Journal of Geotechnical and Geoenvironmental Engineering 2012;138(1):100–9.
Dafalias YF. Bounding surface formulation of soil plasticity, soil mechanics-transient and cyclic loads. Wiley; 1982. p. 253–82.
Dafalias YF. Bounding surface plasticity. I: Mathematical foundation and hypoplasticity. Journal of Engineering Mechanics 1986;112(9):966–87.
Dafalias YF, Popov EP. A model of nonlinearly hardening materials for complex loading. Acta Mechanica 1975;21:173–92.
Dunne F, Petrinic N. Introduction to computational plasticity. New York: Oxford University Press; 2005.
Fjaer E, Holt RM, Horsrud P, Raaen AM, Risnes R. Petroleum related rock mechanics. Amsterdam: Elsevier; 2008.
Fu Z, Chen S, Peng C. Modelling cyclic behaviour of rockfill materials in a framework of generalized plasticity. ASCE International Journal of Geomechanics 2014;14(2):191–204.
Gens A, Nova R. Conceptual bases for a constitutive model for bonded soils and weak rocks. In: Proceedings of the geotechnical engineering of hard soils-soft rocks. Athens; 1993. p. 485–94.
Hashiguchi K. Subloading surface model in unconventional plasticity. International Journal of Solids and Structures 1989;25(8):917–45.
Hashiguchi K, Chen ZP. Elastoplastic constitutive equation of soils with the subloading surface and the rotational hardening. International Journal for Numerical and Analytical Methods in Geomechanics 1998;22(3):197–227.
Imam SMR. Modelling the constitutive behaviour of sand for the analysis of static liquefaction [PhD Thesis]. Edmonton, AB, Canada: University of Alberta; 1999.
Imam SMR, Chan DH. Application of a critical state model for the cyclic loading of sands. In: Proceedings of GeoEdmonton: 61st Canadian geotechnical conference. Edmonton; 2008. p. 127–34.
Imam MR, Morgenstern NR, Robertson PK, Chan DH. Yielding and flow liquefaction of loose sand. Soils Sand Foundations 2002;42(3):19–31.
Imam SMR, Morgenstern NR, Robertson PK, Chan DH. A critical-state constitutive model for liquefiable sand. Canadian Geotechnical Journal 2005;42(3):830–55.
Ishihara K. Liquefaction and flow failure during earthquakes. Géotechnique 1993;43(3):351–415.
Iwan WD. On a class of models for the yielding behaviour of continuous and composite systems. Journal of Applied Mechanics 1967;34(3):612–7.
Jefferies MG. Nor-Sand: a simple critical state model for sand. Geotechnique 1993;43(1):91–103.
Khalili N, Habte MA, Valliappan S. A bounding surface plasticity model for cyclic loading of granular soils. International Journal for Numerical Methods in Engineering 2005;63(14):1939–60.
Khalili N, Habte MA, Valliappan S. Monotonic and cyclic analysis of granular soils. Computational Methods in Engineering & Science 2006:59–70.
Khong CD. Development and numerical evaluation of unified critical state models [PhD Thesis]. Nottingham, UK: University of Nottingham; 2004.
Krieg RD. A practical two-surface plasticity theory. Journal of Applied Mechanics 1975;42(3):641–6.
Lee KH, Chan DH, Lam KC. Constitutive Model for cement treated clay in a critical state frame work. Soils and Foundations 2004;44(3):69–77.
Lenart S. The response of saturated soils to a dynamic load. Acta Geotechnica Slovenica 2008;5(1):37–49.
Ling HI, Yang S. Unified sand model based on the critical state and generalized plasticity. Journal of Engineering Mechanics 2006;132(12):1380–91.

Liu E, Wang S, Zhou C, Nie Q. Mechanical properties of artificial structured soils under a conventional drained loading–unloading–reloading stress path. International Journal of Civil Engineering 2016:1–11.
Manzari MT, Dafalias YF. A critical state two-surface plasticity model for sands. Géotechnique 1997;47(2):255–72.
Marri A. The mechanical behaviour of cemented granular materials at high pressures [PhD Thesis]. Nottingham, UK: University of Nottingham; 2010.
Mohsin AKM. Automated Gmax measurement to explore degradation of artificially cemented carbonate sand [PhD Thesis]. Sydney, NSW, Australia: University of Sydney; 2008.
Mroz Z. On the description of anisotropic workhardening. Journal of the Mechanics and Physics of Solids 1967;15(3):163–75.
Mroz Z, Norris VA, Zienkiewicz OC. An anisotropic hardening model for soils and its application to cyclic loading. International Journal for Numerical and Analytical Methods in Geomechanics 1978;2(3):203–21.
Mroz Z, Norris VA, Zienkiewicz OC. Application of an anisotropic hardening model in the analysis of elastoplastic deformation of soils. Géotechnique 1979;29(1):1–34.
Nova R. A simple elastoplastic model for soils and soft rocks. In Soil Constitutive Models – Evaluation, Selection, and Calibration 2005;128:380–99.
O'Reilly MP, Brown SF. Cyclic loading of soils: from theory to design. Glasgow: Blackie and Son Limited; 1991.
Pastor M, Zienkiewicz OC, Leung KH. Simple model for transient soil loading in earthquake analysis. II. Non-associative models for sands. International Journal for Numerical and Analytical Methods in Geomechanics 1985;9(5):477–98.
Pastor M, Zienkiewicz OC, Chan AHC. Generalized plasticity and the modelling of soil behaviour. International Journal for Numerical and Analytical Methods in Geomechanics 1990;14(3):151–90.
Rahimi M. Constitutive modelling of soft sandstone degradation under cyclic conditions [PhD Thesis]. Edmonton, AB, Canada: University of Alberta; 2014.
Rahimi M, Chan D, Nouri A. Bounding surface constitutive model for cemented sand under monotonic loading. International Journal of Geomechanics 2015;16(2):04015049.
Rahimi M, Chan D, Nouri A, Rasouli R. Effects of inherent fabric anisotropy and intermediate principal stress on constitutive behaviour of uncemented and cemented sands. Computers and Geotechnics 2016;80:237–47.
Rahimi M, Chan D, Nouri A. Constitutive model for cyclic behaviour of cohesionless sands. Geomechanics and Geoengineering 2017;12(1):36–47.
Russell A, Khalili N. A bounding surface plasticity model for sands exhibiting particle crushing. Canadian Geotechnical Journal 2004;41(6):1179–92.
Schnaid F, Prietto PDM, Consoli NC. Characterization of cemented sand in triaxial compression. Journal of Geotechnical and Geoenvironmental Engineering 2001;127(10):857–68.
Tariq KA, Maki T. Cement treated sand as a measure against cyclic loading. Grouting and Deep Mixing 2012:1985–94.
Vermeer PA, de Borst R. Non-associated plasticity for soils, concrete and rocks. Heron 1984;29(3):1–64.
Weng MC. A generalized plasticity-based model for sandstone considering time-dependent behaviour and wetting deterioration. Rock Mechanics and Rock Engineering 2014;47(4):1197–209.
Weng MC, Ling HI. Modelling the behaviour of sandstone based on generalized plasticity concept. International Journal for Numerical and Analytical Methods in Geomechanics 2012;37(14):2154–69.
Wood DM. Soil behaviour and critical state soil mechanics. New York: Cambridge University Press; 1990.
Yang C, Huang MS, Cui YJ. Constitutive model of unsaturated structured soils under cyclic loading. In: Proceedings of the 5th international conference on unsaturated soils; 2011. p. 987–92.
Yoshinaka R, Tran TV, Osada M. Non-linear, stress- and strain-dependent behaviour of soft rocks under cyclic triaxial conditions. International Journal of Rock Mechanics and Mining Sciences 1998;35(7):941–55.
Yu HS, Tan SM, Schnaid F. A critical state framework for modelling bonded geomaterials. Geomechanics and Geoengineering 2007;2(1):61–74.
Yu HS. Plasticity and geotechnics. New York: Springer; 2006.
Zhang K, Zhou H, Shao J. An experimental investigation and an elastoplastic constitutive model for a porous rock. Rock Mechanics and Rock Engineering 2013;46(6):1499–511.
Zienkiewicz OC, Leung KH, Pastor M. Simple model for transient soil loading in earthquake analysis. I. Basic model and its application. International Journal for Numerical and Analytical Methods in Geomechanics 1985;9(5):453–76.

Dr. Mojtaba Rahimi is currently an assistant professor at the Department of Mechasssnical Engineering of the Azad University of Khomeinishahr. He earned a BSc degree in mining engineering from the University of Birjand in 2006 as the first rank graduate. His major during MSc period was in petroleum reservoir engineering. Mojtaba obtained his MSc degree from the Sharif University of Technology, the most prestigious and competitive university in Iran, in 2009. Then, he joined the School of Mining and Petroleum Engineering of the University of Alberta in 2009. Petroleum geomechanics with focus on the constitutive modelling of uncemented and cemented sands was his research topic during the PhD period. Mojtaba worked under supervision of Prof. Dave Chan and Prof. Alireza Nouri during his PhD study and earned a PhD degree from the University of Alberta in 2014. Mojtaba's PhD research has so far led to publication in four SCI journals. He also had a short postdoc period in the University of Saskatchewan under supervision of Prof. Chris Hawkes in 2014. During his postdoc period, Mojtaba worked in area of petroleum geomechanics specifically on effects of stress induced anisotropy and inherent anisotropy on response of sonic logging tools.